Generation of silver-anatase nanocomposite by excimer laser-assisted processing

Cite as: AIP Advances **2**, 032171 (2012); https://doi.org/10.1063/1.4754284
Submitted: 26 May 2012 • Accepted: 07 September 2012 • Published Online: 17 September 2012

Yasir F. Joya, Zhu Liu and Zengbo Wang

Generation of silver-anatase nanocomposite by excimer laser-assisted processing

Yasir F. Joya,[1,a] Zhu Liu,[1] and Zengbo Wang[2]
[1]*Corrosion and Protection Centre, The Mill, School of Materials, The University of Manchester, Manchester M13 9PL, United Kingdom*
[2]*School of Electronic Engineering, Bangor University, Dean Street, Bangor, Gwynedd LL57 1UT, United Kingdom*

(Received 26 May 2012; accepted 7 September 2012; published online 17 September 2012)

We demonstrate crystallization of the anatase thin film with self-adhering silver nanoparticles (Ag NPs) by a single-step laser process. Titanium dioxide (TiO_2) sol-gel precursor film was deposited on glass substrate and Ag ions were adsorbed from silver nitrate aqueous solution. A nanosecond (ns) pulsed beam of KrF (248 nm) laser was traversed across the amorphous Ag-TiO_2 film leading to crystallization of the anatase and simultaneous generation of cubic as well as hexagonal Ag NPs. A uniform size distribution of Ag NPs was observed with an average size of 9.6 nm. On the other hand, anatase grains were 38 nm in size as determined by X-ray diffraction (XRD) and scanning transmission electron microscope (STEM). Analytical simulations indicated a solid-state diffusion and phase transformation mechanism dominating within the film due to laser treatment. [http://dx.doi.org/10.1063/1.4754284]

I. INTRODUCTION

Materials based on the anatase phase of TiO_2 semiconductor have been widely used for various photo-catalytic applications owning to their low cost, chemical and biological inertness, non-toxicity etc. However, the anatase may not respond to light excitations within the visible region due to its wide energy band gap (3.3 eV $\sim$ 386 nm), and thus absorbs only a fraction of the solar spectrum.[1,2] However, due to its amazing properties and economy, it is desired to extend its applications domain from ultraviolet to visible region (400-700 nm). For this purpose, plenty of research has been pursued to generate anatase in the form of nanoparticles, nanotubes and nanowires etc. However, these efforts could not lead to a much significant improvement in photo-catalytic properties of the anatase.[3,4]

An alternate strategy was to load noble (Ag, Pt, Au) metallic species within the anatase, and this proved to be quite successful in promoting the photo-catalytic performance under the visible light.[4–6] Ag NPs possess a quality of high photo-absorption in the visible region owing to the surface plasmon resonance (SPR) effect.[7] Therefore, a worldwide research interest has been developed to synthesize nanocomposite structures consisting of silver-anatase (Ag-TiO_2) for various photo-catalytic as well as antibacterial applications.[8–11] In this instance, generally photo-chemical and thermo-physical methods have been adopted.[12,13]

In a typical photo-chemical process, Ag ions are directly adsorbed on anatase film/nanoparticles from their aqueous solution and photo-chemically reduced into metallic state.[14] This involves extensive pre/post-processing steps e.g. furnace heating cycles and UV light exposure, which also restricts the deposition of Ag-TiO_2 film on lower melting substrate such as polymers and plastics. A flexible and time efficient process has always been desired for developing uniform Ag-TiO_2 nanocomposite structures with required properties on variety of substrates.

[a]Author (The Corresponding Author) is currently working at the Centre for Advanced Studies in Physics, Government College University Lahore, 1-Church Road, Lahore 54000, Pakistan. Email: yasir.joya@outlook.com

TABLE I. The laser operating window for processing of Ag-TiO_2 thin film.

Laser	Wavelength, nm pulse width, ns	Rep. Rate, Hz	Fluence, mJ/cm^2	No. of pulses
GSI Lumonics KrF laser (80 W)	248, 13-20	15	80-90	50-200

FIG. 1. A typical ELAP setup for treatment of Ag-TiO_2 thin films, inset shows the GSI excimer laser system.

We have published on a sol-gel/laser-induced technique to prepare nanocrystalline anatase-based films on glass.[15–17] In the present research, we have applied a quite similar excimer laser-assisted process (ELAP) to modify Ag-TiO_2 films on the glass substrate. By this approach, plain TiO_2 films with self-adsorbed Ag^{2+}/Ag^{1+} ions were successfully transformed into nanocrystalline silver-anatase nanocomposite structure by pulsed ultraviolet laser beam. It combines the benefit of both photo-thermal and photo-chemical phenomenon in a single-step and thus saves considerable time and effort. In addition, the process is conducted at room temperature because there is no requirement for high temperature equipment.

II. EXPERIMENTAL

The recipe for making sol-gel TiO_2 precursor film was acquired from our previous work.[18] As-dried TiO_2 precursor films were immersed into a silver nitrate ($AgNO_3$, 0.01M) aqueous solution for 15 minutes. Films were subsequently rinsed with de-ionized water (DI) and dried in air. A pulsed KrF excimer laser was irradiated on the film at optimized parameters as listed in Table I. Excimer laser keeps a rectangular beam shape and top-hat profile, however, it is essential to use more uniform central portion of the raw beam to increase reproducibility of results. The laser beam size was reduced to 5×5 mm^2 on the sample for this purpose, which was obtained by masking inhomogeneous edges of the raw beam through a steel aperture. A typical experimental arrangement for ELAP treatment is shown in Fig. 1.

The crystalline structure of films before and after laser irradiation was determined by XRD (Philips X'pert-APD grazing incidence angle XRD machine). Spectra were obtained from 20-70° 2theta with a step size of 0.05 and scan time/step of 6 seconds. A glancing angle of 4° was selected to increase the signals from the thin film. The anatase grain size was calculated from Scherrer's

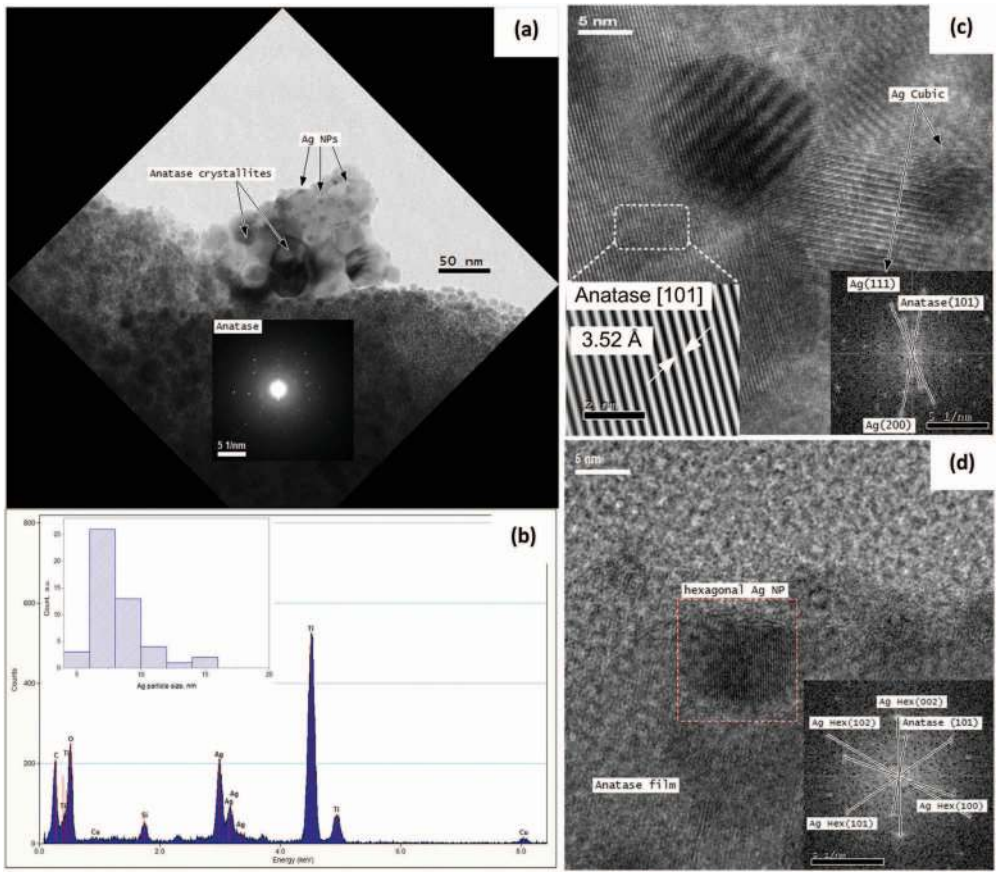

FIG. 2. STEM image of Ag-TiO_2 thin film fragment (inset is a SAED pattern) after 50 laser pulses at 85 mJ/cm^2 (a) a corresponding EDX with inset showing the Ag NPs size distribution histogram (b) HRTEM images with relative FFT insets of cubic and hexagonal Ag NPs (c) and (d).

method by using the following relation.

$$D = \frac{0.9\lambda}{BCos\theta_b} \tag{1}$$

Where, *'D'* is the average particle size in angstroms, *'B'* is the width of the peak at half the peak height in radians, *'λ'* is the X-ray wavelength in angstroms, and θ_b is the Bragg's angle in degrees. Analytical simulation of temperature induced by a single laser pulse interaction with plain TiO_2 film was compiled and run in Wolfram Mathematica (8.0.1). A one-dimensional heat equation model was used for this purpose to simply complex calculations. Nanostructure imaging at high resolution and chemical analysis was carried out by STEM coupled with EDX detector and selected area electron diffraction (SAED). Sample for STEM was prepared by immersing the film in DI water and scraping off fragments, which were picked on carbon-coated grid and dried on filter paper in the oven at 80°C before examination.

III. RESULTS AND DISCUSSIONS

A. Imaging and Chemical Analysis by STEM

A STEM image obtained from Ag-TiO_2 film fragment after 50 laser pulses at 85 mJ/cm^2 fluence is shown in Fig. 2. It reveals distinct areas consisting of a matrix phase (light) and a dispersion of Ag NPs (dark) over it. The SAED from corresponding area revealed a crystalline pattern as shown by the inset in Fig. 2(a), which closely matched with the anatase (JCPDS-00-21-1272) phase of TiO_2.

Moreover, an EDX line scan performed across the film produced strong signals from Ag, Ti and O confirming the Ag NPs formation during the laser treatment. Additional peaks of C, Si and Cu originated from the carbon film and STEM sample grid.

By close observation, the anatase grains were sintered together at edges and Ag NPs were self-adhering to the anatase grains. Roughly, an average grain size of 38 nm was obtained from the anatase, whereas Ag NPs were approximately 9.6 nm across as determined from STEM image. Ag NPs size distribution was verified by performing an image analysis and plotting a histogram as shown in Fig. 2(b) inset. It is evident that most of the Ag NPs synthesized by ELAP were within 5-10 nm range.

High resolution TEM (HRTEM) images obtained from the same Ag-TiO_2 film are shown in Figs. 2(c) and 2(d). The lattice fringes are visible in the matrix and correspond to (101) plane of the anatase (JCPDS-00-21-1272) as shown by HRTEM filter image in Fig. 2(c) inset. The particles appearing in dark shade (arrow and square) were identified by their corresponding FFT and revealed a cubic (JCPDS- 01-071-4613) as well as hexagonal (JCPDS- 01-071-5025) crystal structure as shown in Figs. 2(c) and 2(d) insets. A crystallite size of cubic silver NP as-observed from HRTEM image was approximately 8.5 nm, whereas hexagonal crystal was 11 nm across its edges.

The ultraviolet laser treatment of Ag-TiO_2 film leads to a promising solution to develop silver-anatase nano-composites on glass or glazed surfaces. However, certain aspects still remain to be further investigated to explain dual symmetries of Ag NPs after laser irradiation. Generally, it may be ascribed to non-equilibrium phase transformation by the laser interaction with Ag ions or other processing factors. The silver-anatase structure is generated at optimized laser fluence i.e. 85 mJ/cm^2 with 50 shots at 15 pulses/sec repetition rate in order to suppress the rutile formation. However, effect of laser parameters on Ag NPs generation and transformation needs further steps of experiments and characterization.

B. XRD Analysis and the Crystallite Size

XRD results of the plainTiO_2 and Ag-TiO_2 films before and after ELAP are shown in Fig. 3. The as-dried TiO_2 film (350°C, 30 minutes) exhibited a halo curve shape indicating amorphous state. However, several crystallographic peaks were generated after irradiation with 50 laser pulses at 85 mJ/cm^2 fluence. The d-spacing values obtained from various peaks corresponded to the anatase phase of TiO_2 (JCPDS-00-21-1272). Additional peak at 27.8 degrees was associated with the rutile phase of TiO_2 (JCPDS-00-21-1276). On the other hand, Ag-TiO_2 film prepared at the same parameters, revealed anatase structure without any mixing of the rutile phase. In this sample, intensity of (101) planes of the anatase was greater than the plain TiO_2, which indicates that a greater crystallization volume of anatase was obtained in the former after ELAP.

The excimer laser keeps a very short pulse of 13-20 ns only and a total interaction time of 50 pulses equals 1000 ns, which is still quite low from materials point of view. This narrow laser-material interaction is responsible for a very narrow heat affected zone (HAZ) and thermal diffusion is limited. This may in part explain the reason of lower crystallization volume of the anatase in plain TiO_2 film. Whereas, a higher degree of crystallization in Ag-TiO_2 film can be associated with higher thermal conductivity of Ag NPs compared to plain TiO_2, which aided photo-thermal diffusion induced by the laser into the anatase matrix.

Moreover, a stabilization effect to formation of the anatase was revealed by Ag-TiO_2 film after the laser irradiation. When the laser pulses were increased up to 200 at 85 mJ/cm^2 fluence, the anatase was still observed to be dominant as indicated in our previous report.[19] It may be attributed to the laser absorption by Ag NPs in addition to TiO_2 resulting in laser energy distribution among these species and thus less energy was available to the anatase for phase transformation. Furthermore, Ag NPs may also induce a pinning effect to growth of the anatase by distributing alongside the grain boundaries of TiO_2 under influence of the laser.

The anatase grain size obtained from various films is listed in Table II. A larger crystallite size obtained in plain TiO_2 film is due to significant anatase grain growth and subsequent transformation

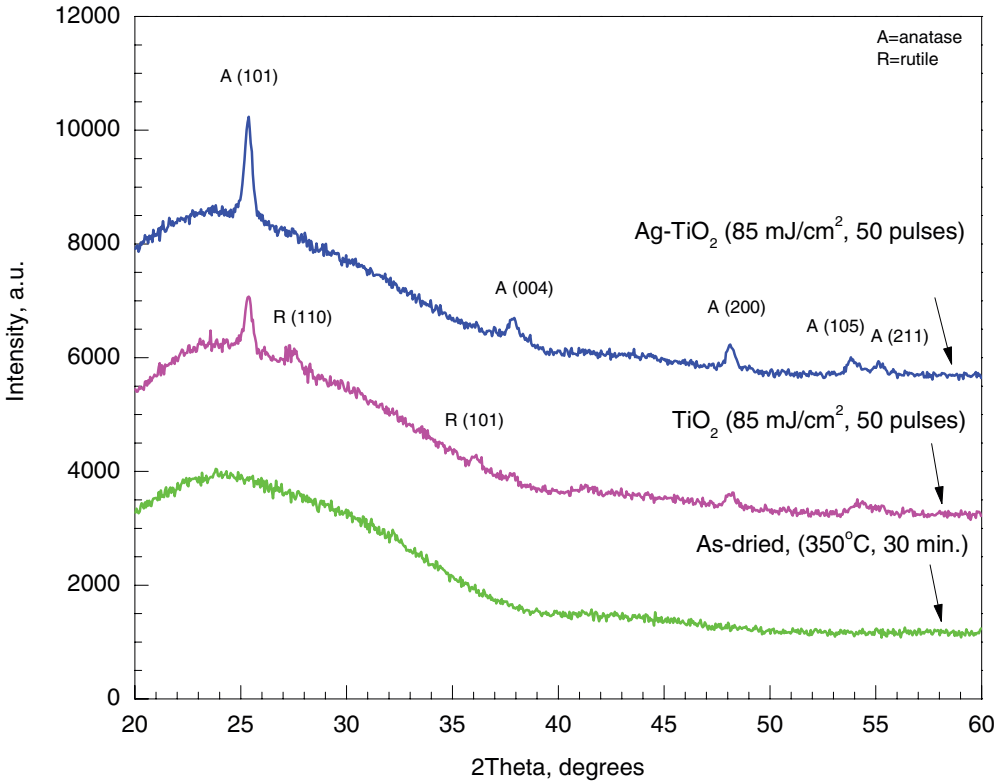

FIG. 3. XRD spectra of plain TiO_2 and Ag-TiO_2 thin film before and after ELAP treatment.

TABLE II. Anatase grain size obtained from various TiO_2 films by XRD.

Sample	Identified phase	(h k l) plane	Crystallite size, nm
TiO_2 by ELAP	Anatase+Rutile	(101)	43.1
Ag-TiO_2 by ELAP	Anatase	(101)	38.4

into the rutile phase. The anatase grain size (38.4 nm) is quite close to STEM observations (40 nm). A slight difference may result from the machine intrinsic broadening and may be neglected.

C. Numerical Simulation

It is well known that crystallization is a thermo-physical phenomenon, which is dependent on the surrounding temperature of the material. A nanosecond laser-material interaction is more specialized case in which temperature is generated by laser-induced excitations at the atomic level.[20] In the present study, incident high energy photons may trigger thermal as well as photochemical modification within amorphous TiO_2 film. Generally, crystallization of the anatase requires a temperature exceeding 400°C by thermal and/or photo-thermal mechanism. However, ultraviolet photons of the excimer laser are capable to introduce photochemical transformation inside the film at room temperature.

Here, we will consider a 350 nm deep plain TiO_2 film on glass to numerically simulate the photo-thermal changes. The temperature attained during interaction of a 13 ns laser pulse with the film surface can be calculated by solving the standard three-dimensional heat equation. However, for large area irradiation (unfocussed), the temperature remains more or less uniform within z plane

TABLE III. Standard thermo-physical data of TiO_2 used for numerical simulation.

TiO_2 at 25°C	[Refs. 2, 23]
ρ *(g/cm^3)*	3.8
C_p *(J/g K)*	0.69
k_c *(W/cm K)*	0.065
α *(/cm)*	710000
R (Reflectance)	0.28

and the temperature rise can be calculated by one-dimensional heat equation.[21,22]

$$c_p \rho \frac{\partial T(z,t)}{\partial t} = \frac{\partial}{\partial z}[k_c \frac{\partial T(z,t)}{\partial z}] + \alpha I(z,t) \tag{2}$$

$$I(z,t) = I_0(t)(1-R)e^{-\alpha z} \tag{3}$$

$$I_0(t) = I_0[\frac{t}{\tau}]^{\beta} \exp\left[\beta(1-\frac{t}{\tau})\right] \tag{4}$$

Where, 'β' determines the temporal pulse shape, 'z' the depth of film in *nm*, 't' the time in *ns*, 'τ' the laser pulse width in *ns*, 'T' the temperature in °C, 'c_p' the specific heat, 'k_c' the thermal conductivity, 'α' the absorption coefficient,'R' the reflectance and 'ρ' the density of TiO_2 film. Standard thermo-physical properties of TiO_2 anatase were used against each of these parameters where feasible as shown in Table III.

Equation (2) was numerically solved to calculate the temperature rise and supplemented with specific boundary conditions to obtain the final surface temperature as follows.

$$T_{TiO_2} = 273 + T(x,y,z,t) \quad at\ \mathrm{t} = 0\,\mathrm{s} \quad \text{and} \quad \mathrm{z} = 0\ \mathrm{nm} \tag{5}$$

Simulation results of calculated temperature against the laser pulse interaction time are plotted in Fig. 4(a). The inset shows an exaggerated part of the curve near the peak temperature and differentiates between various applied fluence values. Results indicate that a peak surface temperature of 852, 941 and 1030°C is generated at the surface of plain TiO_2 film after interaction with a single laser pulse at 65, 75 and 85 mJ/cm^2 fluence respectively. The temperature levels off quickly to 400°C after 100 ns due to a very short interaction time of the laser pulse. In addition, temperature variations across the film thickness after a single laser pulse at varying fluence are shown in Fig. 4(b). It reveals that by 85 mJ/cm^2 laser fluence, a thermal field is generated that diffuses as deep as 350 nm into the material, which is also the thickness of TiO_2 film, but the temperature drops to 439°C at that point. A smooth thermal gradient is thus set up during interaction of a single pulse of the excimer laser with TiO_2 film.

Interestingly, for all intensities, calculated peak temperature remained well below the melting point (1870°C) of TiO_2 film.[2] The excimer laser melting threshold of TiO_2 film has been reported to occur at 250 mJ/cm^2 fluence according to a recent study.[24] It can therefore be established that there was no melting or ablation of TiO_2 during the ELAP treatment at 85 mJ/cm^2 fluence. However, the temperatures are significantly high and coincide with the sintering temperature of TiO_2, which is promoted by solid-state diffusion. Although, sintering temperature lies within the rutile stability range, anatase is still crystallized as a dominant phase after ELAP treatment as witnessed by XRD and STEM results. The effect of multiple laser pulses and interaction with Ag NPs cannot be accomplished due to the present software limitations. However, a more detailed discussion on this topic will follow in our next publication.

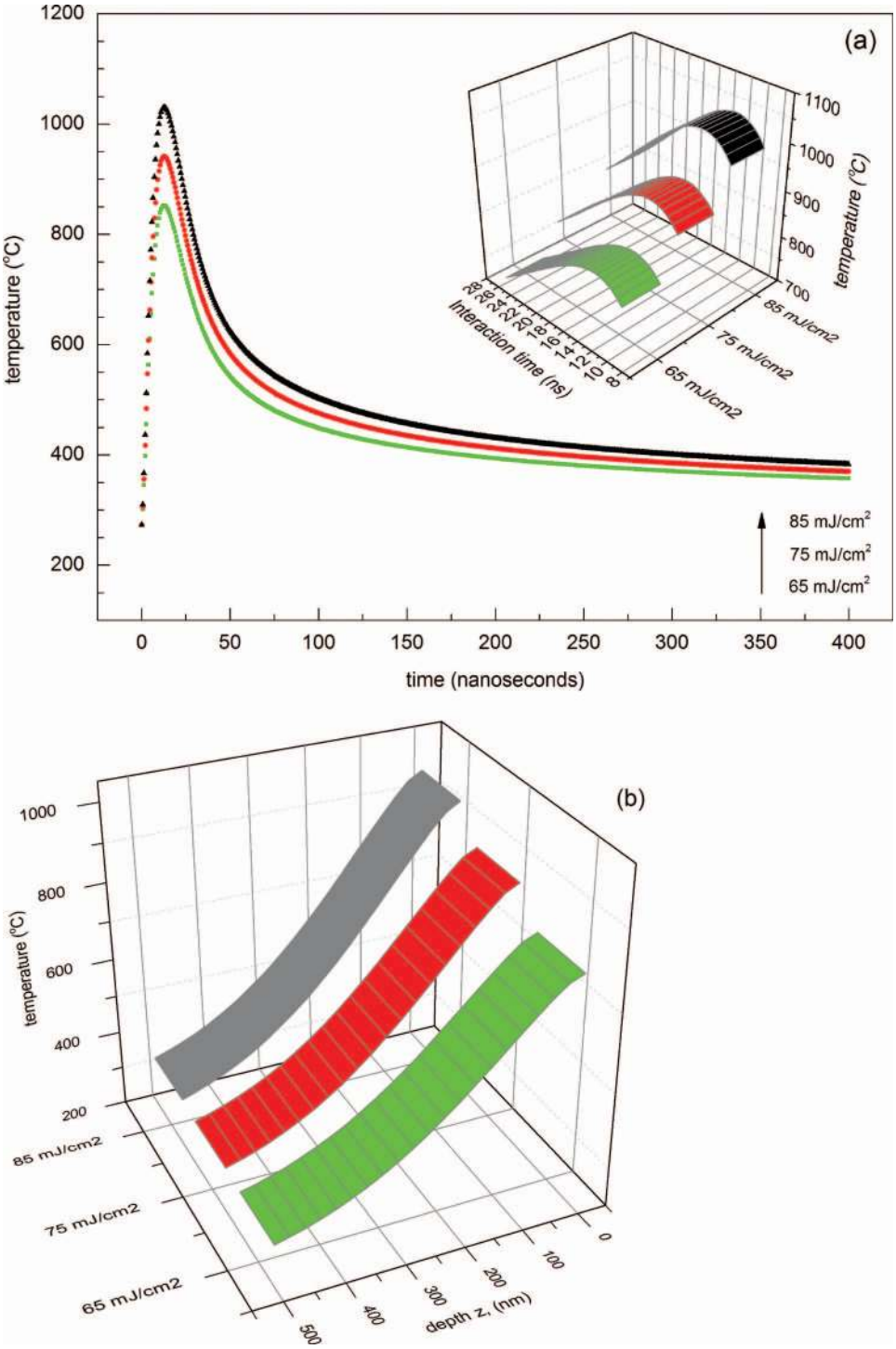

FIG. 4. Numerical simulation of temperatures attained during a single laser pulse interaction with TiO_2 film surface a) and across the depth b) at a range of laser fluence.

IV. CONCLUSIONS

In summary, nanocrystalline silver-anatase nanocomposite thin films were successfully developed on glass by ELAP treatment. Laser energy and the number of pulses were optimized to avoid melting/ablation yet to increase the temperature of Ag-TiO_2 film photo-thermally to crystallization

and sintering of the anatase. At the same time, silver ions were reduced and metallized photochemically into Ag NPs. The photothermo-chemical transformation can be flexibly customized by changing laser parameters to obtain the desired ratio of constituents (anatase, rutile etc.). Both cubic as well as hexagonal silver crystals were formed and a uniform size distribution was achieved by ELAP without any surfactants. Crystallization of the anatase during laser irradiation was significantly improved with silver addition compared to the plain TiO_2. This is a new advance in laser processing for photochemical generation of NPs, which may lead to UV laser-assisted metallization of metal NPs on various substrates especially in photovoltaic devices.

ACKNOWLEDGMENT

Authors would like to acknowledge the Higher Education Commission (HEC), Government of Pakistan for sponsoring this research and staff at School of Materials, the University of Manchester for their help in using various machines for characterization.

[1] K. Hashimoto, H. Irie, and A. Fujishima, Japanese Journal of Applied Physics Part 1-Regular Papers Brief Communications & Review Papers **44**, 8269 (2005).
[2] U. Diebold, Surf. Sci. Rep. **48**, 53 (2003).
[3] X. Chen and S. S. Mao, Chemical Reviews **107**, 2891 (2007).
[4] T. Kemp and R. McIntyre, Polymer Degradation and Stability **91**, 3010 (2006).
[5] J. Yu, J. Xiong, B. Cheng, and S. Liu, Applied Catalysis B-Environmental 211 (2005).
[6] J. He, I. Ichinose, T. Kunitake, and A. Nakao, Langmuir **18**, 10005 (2002).
[7] J. Millstone, S. Hurst, G. Metraux, J. Cutler, and C. Mirkin, Small **5**, 646 (2009).
[8] R. Kumar and G. Raza, Ionics 579 (2009).
[9] K. Page, R. Palgrave, I. Parkin, M. Wilson, S. Savin, and A. Chadwick, J. Mater. Chem. 95 (2007).
[10] N. Crespo-Monteiro, N. Destouches, L. Nadar, S. Reynaud, F. Vocanson, and J. Y. Michalon, Appl. Phys. Lett. **99**, 173106–3 (2011).
[11] S.-J. Lin, K.-C. Lee, J.-L. Wu, and J.-Y. Wu, Appl. Phys. Lett. **99**, 043306–3 (2011).
[12] X. He, X. Zhao, and B. Liu, Journal of Non-Crystalline Solids **354**, 1267 (2008).
[13] J. T. A. Ahmad and S. Ismat Shah, Journal of Physics: Conference Series **61**, 11 (2007).
[14] Y. Ohko, T. Tatsuma, T. Fujii, K. Naoi, C. Niwa, Y. Kubota, and A. Fujishima, Nature Mater. **2**, 29 (2003).
[15] Y. F. Joya and Z. Liu, Scrip. Mater. **60**, 467 (2009).
[16] Y. F. Joya and Z. Liu, J. Optoelec. Adv. Mater. **12**, 589 (2010).
[17] Y. Joya and Z. Liu, J. Appl. Phys. A-Mater. Sci. & Proc. **102**, 91 (2011).
[18] Y. F. Joya, T. Wang, and Z. Liu, in ICALEO, Florida, USA. 1152 (2011).
[19] Y. Joya, Z. Liu, and T. Wang, Appl. Phys. B: Lasers & Optics **105**, 525 (2011).
[20] J. C. Ion, *Laser Processing of Engineering Materials, principles, procedure and industrial application 1st ed.* (Elsevier Butterworth-Heinemann, Oxford, 2005), p. 142.
[21] D. Bauerle, *Laser Processing and Chemistry* 4th Ed. (Springer-Verlag Berlin Heidelberg, 2011), p. 111.
[22] J. Rhee, S. Kim, C. W. Sterner, J. O. White, and S. G. Bishop, J Appl. Phys. **90**, 2760 (2001).
[23] E. D. Palik, *Handbook of Optical Constants of Solids* (Elsevier, Academic Press, London, 1998), p. 799. Also see http://refractiveindex.info/.
[24] O. Van Overschelde, T. Delsate, and R. Snyders, J. Appl. Phys. **111**, 123108 (2012).